JOURNAL OF AIRCRAFT
Vol. 42, No. 5, September–October 2005

Active Control of Flow Separation from Supercritical Airfoil Leading-Edge Flap Shoulder

LaTunia Pack Melton,* Norman W. Schaeffler,† and Chung-Sheng Yao‡
NASA Langley Research Center, Hampton, Virginia 23681
and
Avi Seifert§
Tel-Aviv University, 69978 Ramat-Aviv, Israel

Zero-net mass-flux periodic excitation was applied at the leading-edge flap shoulder of a simplified high-lift airfoil to delay flow separation. The term simplified infers that no slat or Fowler flaps are used. The NASA energy efficient transport supercritical airfoil was fitted with a 15% chord simply hinged leading-edge flap and a 25% chord simply hinged trailing-edge flap. Initially, the cruise configuration data from previous experiments were reproduced. The effects of leading- and trailing-edge flap deflections on the airfoil integral parameters were quantified. Detailed flow features were measured to identify optimal actuator placement. The measurements included steady and unsteady model and tunnel wall pressures, wake surveys, arrays of surface hot films, flow visualization, and particle image velocimetry. Eventually, high-frequency periodic excitation was applied to delay the occurrence of leading-edge flap shoulder stall and increased the maximum lift by 10–15%. Low-frequency amplitude modulation was used to reduce the oscillatory momentum coefficient by roughly 50% with similar aerodynamic performance gains. It is demonstrated that the efficacy of the amplitude-modulated excitation is due to the generation of low-frequency motion, which is amplified by the separating shear layer.

Nomenclature

C_{dp} = pressure drag coefficient
C_L = lift coefficient
$C_{L,\max}$ = maximum lift coefficient
C_p = wall pressure coefficient, $(P - P_s)/q$
$C_{p,\min}$ = minimum pressure coefficient
C_μ = oscillatory blowing momentum coefficient, J'/cq
c = model chord
F^+ = reduced frequency, $(f x_{\mathrm{sp}})/U_\infty$
f = oscillation frequency, Hz
h = slot height or width
J' = momentum at slot exit, $\rho h u_j^2$
M = Mach number
P = pressure
q = freestream dynamic pressure, $1/2\rho U_\infty^2$
Re_c = chord Reynolds number, $U_\infty c/\nu$
T = temperature
U = averaged streamwise velocity
u = standard deviation of fluctuating streamwise velocity
x/c = normalized streamwise location
z = spanwise location
α = angle of attack
δ_f = trailing-edge flap deflection
δ_s = leading-edge flap deflection
ν = kinematic viscosity
ρ = density

Subscripts

b = baseline flow conditions
c = cavity
j = conditions at blowing slot
∞ = freestream conditions

Superscript

$'$ = root mean square of fluctuating value

Presented as Paper 2002-3156 at the 1st Flow Control Conference, St. Louis, MO, 24–26 June 2002; received 21 April 2004; revision received 23 September 2004; accepted for publication 30 September 2004.

*Research Engineer, Flow Physics and Control Branch, MS 170; l.p.melton@larc.nasa.gov. Senior Member AIAA.
†Research Engineer, Flow Physics and Control Branch, MS 170; n.w.schaeffler@larc.nasa.gov. Member AIAA.
‡Research Scientist, Flow Physics and Control Branch, MS 170; c.s.yao@larc.nasa.gov.
§Senior Lecturer, Department of Fluid Mechanics and Heat Transfer, School of Mechanical Engineering, Faculty of Engineering; seifert@eng.tau.ac.il. also Visiting Scientist, National Institute of Aerospace, Hampton, Virginia. Associate Fellow AIAA.

Introduction

PERIODIC excitation has been demonstrated to be very effective in controlling boundary-layer (BL) separation in a series of wind-tunnel experiments, performed at both low[1] and high[2] Reynolds numbers. In addition to being effective for controlling separation, the experiments showed that periodic excitation is significantly more efficient, in terms of the momentum input, than steady momentum transfer methods at controlling separation.[1,2] The efficiency of periodic excitation is attributed to the excitation frequencies coinciding with natural instabilities of the separating shear layer. The method was shown to be independent of the BL state, and very high levels of efficiency can be achieved with zero-net mass-flux (ZNMF) actuators that require only electrical input to operate.

The results from the experiments by Seifert et al.[1] and Seifert and Pack[2] were used in a systems study performed by McClean et al.[3] The purpose of the study was to assess the benefits of applying separation control on a passenger transport airplane operating at high subsonic speeds. After a wide range of candidate applications were considered, the simplification of conventional multi-element high-lift systems by active flow control (AFC) was identified as a prime candidate. If the slots and the Fowler effect used on existing high-lift systems were replaced by a simply hinged leading- and trailing-edge flap AFC-enabled system, the overall savings were deemed significant. The AFC is expected to act in a manner similar to the steady jets issuing from the slat and Fowler flap slots in energizing the BL and delaying its separation. The potential benefits included a

0.66% airplane manufacturing cost reduction, up to a 2.8% weight reduction, and about a 3.1% cruise drag reduction, where 1% of the cruise drag reduction was attributable to the elimination of the large, drag-producing external flap hinges and positioning actuators. These benefits are based on an AFC-enabled high-lift system with matching performance of a conventional multi-element high-lift system. The large flap deflection requirements of the simply hinged system necessitate the use of periodic excitation at the leading- and trailing-edge flap shoulders for separation control.

The aforementioned systems study[3] also pointed out the lack of data available on the effectiveness of AFC with a drooped or simply hinged, leading-edge (LE) flap. The purpose of this paper is to provide information on the effectiveness of periodic excitation for controlling separation at the LE flap shoulder of a supercritical airfoil with a drooped nose. The transonic airfoil chosen for the study is the energy efficient transport (EET). This airfoil was chosen because there is an extensive existing experimental and computational database on the three-element version of the model for comparison.[4] Furthermore, the majority of previous AFC studies were not conducted on supercritical airfoils, whereas this study is focused on the high-lift systems of high-subsonic cruise-speed airplanes. This study is, to the best of our knowledge, the first attempt at actively controlling separation from the LE flap shoulder of a supercritical airfoil. The current design completely eliminates hinges and positioning actuators that are external to the airfoil contour, as well as slots between airfoil elements, for energizing the BL. Adding AFC to the design of Ref. 4 was not attempted because it further complicates a complex system, whereas the benefits are expected to be marginal at best.

The present paper begins with a description of the baseline airfoil performance. This stage is a prerequisite to effective placement of actuators, preferably as close to and upstream of the separation location at conditions relevant to high-lift generation. The data acquired to support the determination of the appropriate actuator placement will be discussed. Thereafter, the performance benefits from the activation of the LE flap (LEF) actuator are described and discussed, with emphasis on efficiency considerations.

Experiment

Wind Tunnel

The test was conducted in the Basic Aerodynamic Research Tunnel (BART) at NASA Langley Research Center. The BART facility is a low-speed open-circuit wind tunnel, with a 0.71-m high by 1.02-m wide by 3.05-m long test section. The maximum speed of the tunnel is 60 m/s ($Re/m = 0.345 \times 10^6$). The wind tunnel is well instrumented and allows optical access for the performance of particle image velocimetry (PIV).

Simplified High-Lift Model

The simplified high-lift version of the NASA EET model[4] was designed in a modular manner so that ZNMF actuators could replace solid regions in the model near the LEF and trailing-edge-flap shoulders (Fig. 1a). This paper will focus on results obtained when periodic excitation is introduced near the LEF shoulder. The 406.4-mm chord model has a 15% chord LEF that can be deflected from 0 to −30 deg and a 25% chord trailing-edge flap (TEF) that can be deflected from 0 to 60 deg. Angle-of-attack settings for the airfoil, the TEF, and the LEF were all automated and computer controlled. The model has 78 streamwise static pressure taps located at midspan and two rows of 18 spanwise static pressure taps spaced 50.8 mm apart, located at $x/c = 0.35$ and 0.94. In addition to the static pressure taps, there are nine unsteady pressure transducers on the model surface (Fig. 1b) and two unsteady pressure transducers embedded in the LE actuator cavity for monitoring the pressure fluctuations produced by the actuator and for correlating the wind-tunnel experiment with the bench-top actuator calibration tests. Pressure belts were placed on the floor and ceiling (when the glass ceiling in is place) of the tunnel to gather wall pressure data that could be used for wind-tunnel wall interference correction. However, the data presented herein have not been corrected for wind-tunnel wall interference.

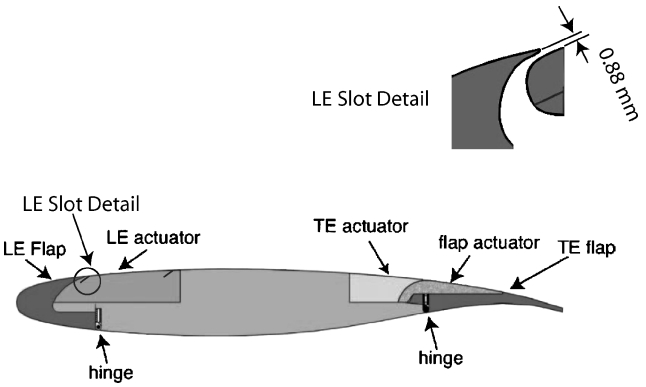

Fig. 1a Modular EET model used for experiment, $c = 406.4$ mm, slots at $x/c = 0.14$ (detail) and 0.30.

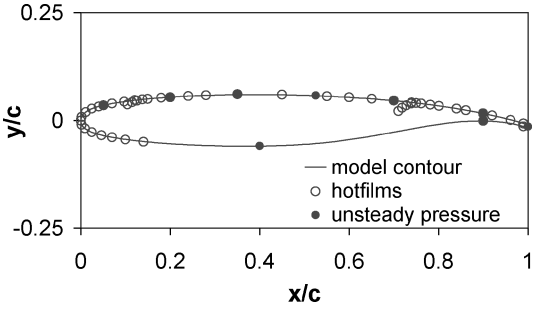

Fig. 1b EET press tap and hot-film locations, $c = 406.4$ mm, LE actuator slots at $x/c = 0.14$ and 0.30.

Hot-Film Arrays

To aid in the determination of the locations of transition and separation, 48 hot films were installed on the model. On each element (LEF, TEF, and main) of the model there are 16 hot-film sensors approximately 50.8 mm to the right of the model centerline, and, therefore, away from the steady pressure tap locations (Fig. 1b). A 16-channel constant temperature anemometer coupled with a switch matrix was used to operate and acquire data from the hot films. The hot films on each element of the model were acquired simultaneously using a 16-bit high-speed analog-to-digital converter. The data were low-pass filtered at 10 kHz and sampled at 25.6 kHz. The films were operated at an overheat ratio of 1.2. The hot-film sensors, 0.4 mm long each, were etched onto a polyimide sheet and then bonded to the model. The polyimide sheet covered one-half of the span of the model. A 0.1-mm step exists at the juncture between the polyimide sheet and the model, and body filler was used to fair the step.

LEF ZNMF Actuator

An internal piezoelectric actuator was placed at the LEF shoulder as shown in Fig. 1a. The actuator had two slots located at $x/c = 0.14$ and 0.3. The slots were inclined approximately 30 deg to the surface, facing downstream, and were 0.88 and 0.5 mm wide, respectively. The forward slot could have been hidden under the LEF at $\delta_s = 0$ deg to eliminate the possible detrimental effects of an exposed slot at cruise if an LEF with a sharper trailing edge (TE) had been fabricated. The $x/c = 0.3$ slot had an alternative cover plate for sealing the slot. A comprehensive bench-top calibration, by the use of a hot wire, was performed on the LE actuator before installation in the tunnel, and unsteady pressure transducers were installed in the actuator's cavity to monitor its operation while in the tunnel. The LE actuator was operated at its resonant frequency f_{res} (853 ± 5 Hz or 1 ± 0.005 kHz, depending on the type of piezoelements installed). Amplitude modulation (AM) at a frequency of an order of magnitude lower than the resonant frequency was used to generate a reduced frequency F^+ of order one. Hot-wire measurements were acquired at spanwise intervals of 254 mm for the 1-kHz resonant case and at spanwise intervals of 127 mm for the 853-Hz resonant case, and the variations in rms velocity were 11 and 25%,

Table 1 Uncertainty of airfoil integral parameters

Parameter	Fully attached	Stalled	Controlled
C_L	0.01	0.04	0.02
C_{dp}	0.002	0.004	0.003
C_D	0.002	0.008	0.006

respectively. The maximum voltage rms applied to the actuator was 45 V for the 853-Hz resonant frequency actuator and 75 V for the 1-kHz resonant frequency actuator. The maximum rms velocity of the 853-Hz resonant actuator, measured at the $x/c = 0.14$ slot during bench-top calibration, was 14 m/s with the $x/c = 0.30$ slot closed and 10 m/s with the $x/c = 0.30$ slot open. The maximum rms velocity of the 1-kHz resonant actuator, measured at the $x/c = 0.14$ slot during bench-top calibration, was 16 m/s with the $x/c = 0.3$ slot closed. For the conditions tested, there were no significant benefits derived from opening both slots of the LE actuator. The peak velocity measured when AM was used corresponds to the peak velocity with pure sine excitation, with the same peak voltage excitation. A sine wave envelope is used for all of the AM data presented.

Flow Visualization

A commercial smoke generator, similar to the type used in theatrical productions, was used to seed the flow with smoke for the flow visualization study performed, as well as for the PIV measurements. The smoke was introduced upstream of the contraction. Video and still photography were used to acquire the images. An argon ion laser was used to form a light sheet.

PIV Setup

Digital PIV was used to measure the instantaneous flowfields, phase synchronized with the LE actuator cycle. The PIV system includes two cameras with resolutions of 1280 by 1024 pixels, equipped with 105-mm macrolens, installed side by side. The field of view from each camera was overlapped to cover both LE actuator slot locations above the airfoil. The magnification of the imaging system was about 9:1, with a measurement plane about 70 mm wide. The interrogation area at each grid point had a 24×24 pixel resolution. This corresponds to about 1.5-mm square at the measurement plane. A maximum overlap of 50% between adjacent interrogation regions was used. Smoke, introduced upstream of the contraction, was used for seeding. Dual Nd–Yag lasers were used to illuminate a light sheet, placed about 50 mm to the left of the model centerline. The laser pulse separation was set at 6–8 μs to cover a freestream velocity of about 30 m/s. For the controlled cases, phase-locked data at 45-deg intervals containing approximately 100 image pairs per phase were acquired. Phase-averaged mean fields and perturbation fields from the phase mean were also estimated.

Experimental Uncertainty

The α presented are accurate to within ± 0.03 deg. The LEF and TEF deflection angles are accurate to within ± 0.25 deg, C_μ is accurate to within 20%, Re_c is accurate to within 3%, and the slot width is accurate to within ± 0.08 mm. The uncertainties of the airfoil integral parameters are listed in Table 1 in absolute values and related to flow conditions.[2]

The large uncertainty in the total drag C_D is due to the extrapolation of the wake data for some of the high-lift configurations of the airfoil.

Discussion of Results

The baseline cruise configuration of the airfoil was tested and compared to previous tests of the same airfoil in a different facility and at a different range of Mach and Reynolds numbers.[4] The data were acquired with the original airfoil contour, before any actuator slots were present (Fig. 1a). The highest available Re_c at BART, 1.5×10^6, is lower than the lowest Re_c tested in the Langley Low Turbulence Pressure Tunnel (LTPT), 2.5×10^6. Figure 2 presents the lift data of the current test and unpublished EET data provided in a private communication by J. C. Lin in 2002. The lift

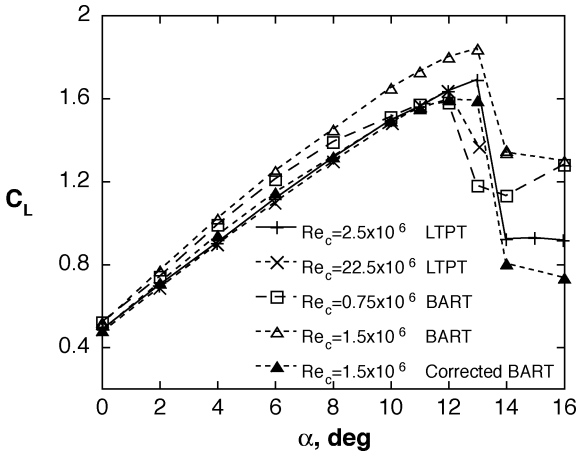

Fig. 2 Comparison of baseline cruise configuration of EET airfoil as tested in BART and LTPT facilities at a range of Reynolds numbers, $\delta_s = \delta_f = 0$ deg.

data indicate that, as expected, significant wall interference exists in the present BART setup. Conventional wind-tunnel wall interference and wake blockage corrections[5] were applied to the data, and the corrected BART lift (for $Re_c = 1.5 \times 10^6$) is in very good agreement with the LTPT data (for $Re_c = 2.5 \times 10^6$) for the cruise configuration (Fig. 2). Weak Re_c effects such as increased lift at low α (due to a laminar separation bubble close to the LE and earlier stall due to a thicker boundary layer) can be seen. However, overall, the reproduction of the LTPT data is satisfactory. Uncorrected lift data measured at BART at $Re_c = 0.75 \times 10^6$ is also shown for comparison and is in good agreement with the higher Re_c data from LTPT and the corrected BART data for $Re_c = 1.5 \times 10^6$. Most of the data to be presented in this paper are for $Re_c = 0.75 \times 10^6$, and it is made certain that turbulent separation would always be considered, minimizing low Re_c effects.

It is expected that wall interference will have a larger influence on the flow as the lift and drag increase, due to LEF and TEF deflections for the high-lift configuration. However, the lift increment and especially the drag reduction with active separation control are expected to be conservative. This is because wind-tunnel interference, at least the wake blockage effect of it, will be reduced because the drag will decrease. Moreover, floor and ceiling pressures were acquired at all flow conditions to assist with future data reduction and with comparison to computational fluid dynamics with the tunnel walls taken into account.

The baseline high-lift characteristics of the simplified high-lift system will now be presented and discussed, including the effect of opening two-dimensional actuator slots in the airfoil upper surface. The purpose of deflecting the LEF was to eliminate the possibility of LE separation, common on supercritical airfoils due to the low radius of curvature of the LE.[6]

Figure 3 shows the effect of deflecting the LEF on the lifting performance of the baseline airfoil at $\delta_f = 0$ deg. The main effect of the LEF deflection is to delay stall to a larger incidence and, therefore, to increase the maximum lift generated by the airfoil. The stall is also milder at larger LEF deflections, alleviating the abrupt stall shown for $\delta_s = 0$ deg. A secondary effect is a somewhat lower lift at low incidence and increased $\mathrm{d}(C_L)/\mathrm{d}(\alpha)$ for the progressively more cambered airfoil, attributed to tunnel interference. The $\delta_s = -30$ deg data are considered an anomaly because stall was not encountered in the available range of α, presumably due to tunnel interference, and, therefore, these data will not be considered. Overall, the LEF has little effect on the prestall lifting performance of the airfoil.

Even though the main focus of this paper is on providing excitation at the LEF shoulder to delay BL separation downstream of the LEF, in application it will be required to consider both LEF and TEF deflections for landing and, to a lesser extent, for takeoff. Figure 4a shows the lift data for a range of TEF deflections at $Re_c = 0.75 \times 10^6$. The typical TEF effect[7] is shown, where the lift is

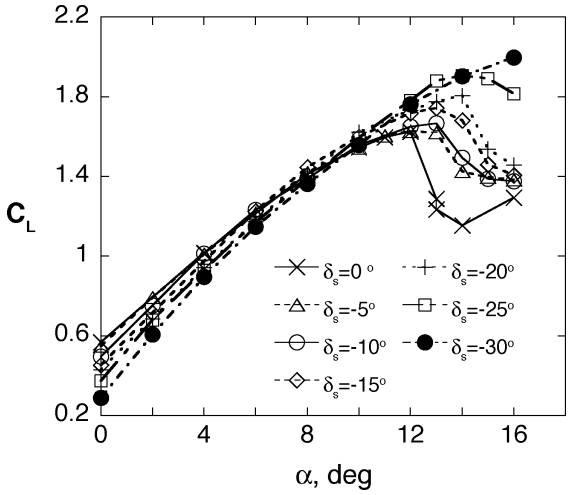

Fig. 3 Lift of the EET airfoil at different LEF deflections δ_s, $Re_c = 0.75 \times 10^6$ and $\delta_f = 0$ deg.

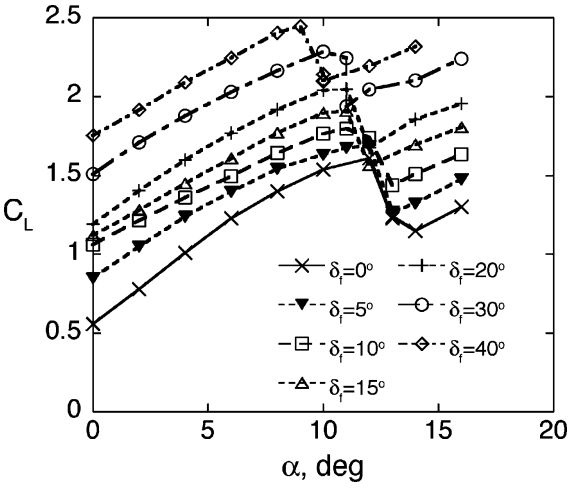

Fig. 4a Lift of EET airfoil at different TEF deflections, $Re_c = 0.75 \times 10^6$ and $\delta_s = 0$ deg.

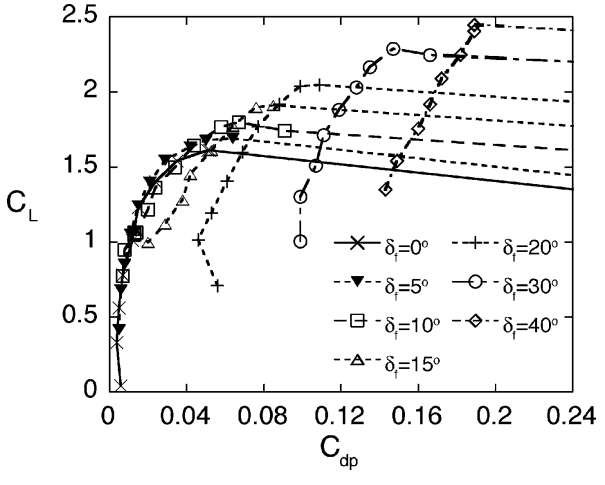

Fig. 4b Lift vs form drag of the EET airfoil at different TEF deflections, $Re_c = 0.75 \times 10^6$ and $\delta_s = 0$ deg.

increased over the entire α range as the TEF is deflected. Figure 4b shows the lift-form-drag data, as well as the TEF effect. From the lift-form-drag data, it is evident that the airfoil with a TEF behaves as a cambered airfoil up to a TEF deflection between 10 and 15 deg, where the lift slope decreases with incidence due to developing TE separation (Fig. 4a). At $\delta_f = 15$ deg, the upper surface is separated from the TEF shoulder downstream, causing a significant drag increase (Fig. 4b) and a constant lift slope (Fig. 4a) before the stall that

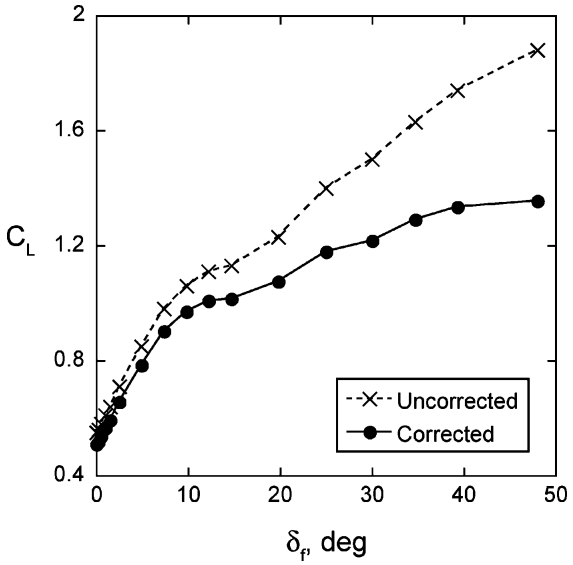

Fig. 4c Corrected and uncorrected lift vs TEF deflection δ_f, $Re_c = 0.75 \times 10^6$, $\delta_s = 0$ deg, and $\alpha = 0$ deg.

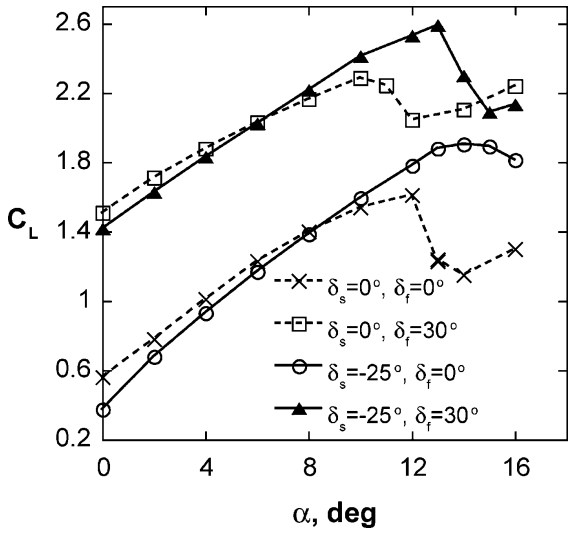

Fig. 5 Lift coefficients of the EET airfoil at different high-lift configurations as tested in BART at $Re_c = 0.75 \times 10^6$.

occurs at progressively smaller incidence as δ_f increases (Fig. 4a). The sudden drop in lift occurs because separation abruptly shifts from the TEF shoulder to the LE.

Figure 4c shows the maximum lift of the TE flapped airfoil at zero LEF deflection and compares it to the corrected maximum lift according to Ref. 5, using the form drag for the wake blockage corrections, because it is not practical to measure wake drag at these highly unsteady separated flow conditions. The corrected TE flapped airfoil lift data show that significant tunnel interference exists, and, as expected, the value of $d(C_L)/d(\delta_f)$ decreases significantly for $\delta_f > 7.5$ deg. Negligible lift increments are obtained for $\delta_f > 35$ deg. However, this could be altered if periodic excitation were applied at the TEF shoulder to increase the suction level there.

The lift coefficient of a candidate flow condition ($\delta_s = -25$ deg and $\delta_f = 30$ deg) for a landing configuration is shown in Fig. 5. The following data are also included in Fig. 5: data for the cruise configuration ($\delta_s = \delta_f = 0$ deg), data for $\delta_s = -25$ deg at $\delta_f = 0$ deg (showing delayed and milder stall), and data for $\delta_f = 30$ deg at $\delta_s = 0$ deg (showing increased lift and earlier, more abrupt stall). The lift data for the $\delta_s = -25$ deg and $\delta_f = 30$ deg configuration indicate that the LEF effect is almost linearly added to the TEF effect and that its stall milding capability is maintained even at $\delta_f = 30$ deg. The challenge is now to apply periodic excitation on both the LEF

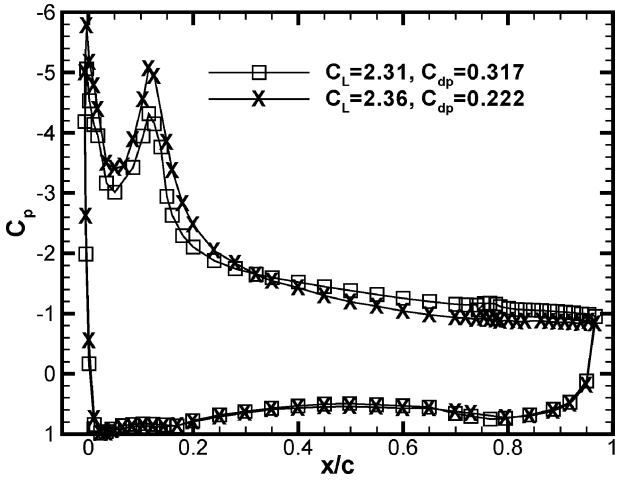

Fig. 6 Comparison of baseline C_p with and without slots on model; model with slots is represented by x, $Re_c = 0.75 \times 10^6$, $\delta_f = 30$ deg, $\delta_s = -25$ deg, and $\alpha = 14$ deg.

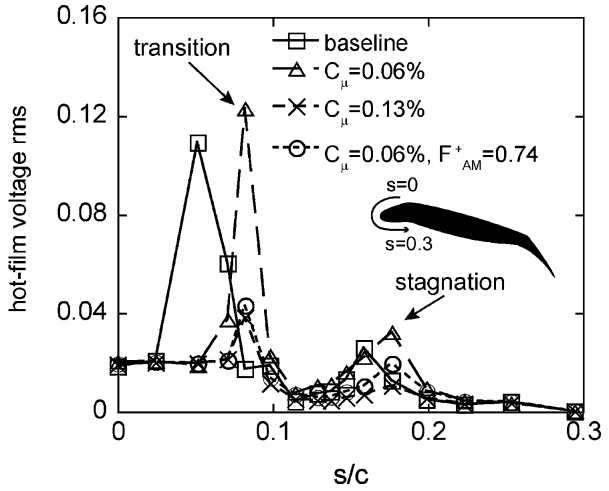

Fig. 7 LE hot-film voltage rms, $\delta_f = 30$ deg, $\delta_s = -25$ deg, $\alpha = 15$ deg, and $Re_c = 0.75 \times 10^6$, $s/c = 0$ is at $x/c = 0.085$ on upper surface, $F^+ = 12.2$ when control applied without AM.

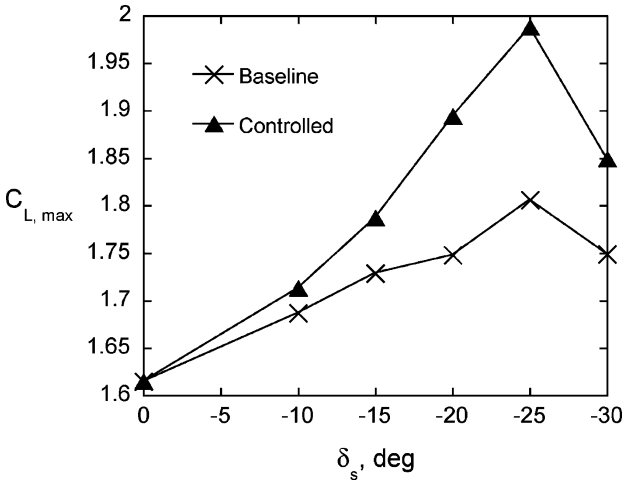

Fig. 8 Effect of LEF deflection on the baseline and controlled maximum lift coefficient, $\delta_f = 4.3$ deg and $Re_c = 0.75 \times 10^6$, both LE actuator slots used $F^+ = 10.5$ and $C_\mu = 0.03\%$.

and TEF shoulders and to delay BL separation at both locations allowing larger LEF and TEF deflections that result in enhanced lift.

In the following paragraphs we shall discuss the effects of slots in the airfoil contour and their effect on the baseline performance, laminar–turbulent BL transition, and, thereafter, the effect of applying periodic excitation at the LEF shoulder. Well-optimized airfoils at relevant Reynolds numbers might suffer performance losses due to the presence of surface discontinuities, such as those created by actuator slots. When AFC is considered for performance improvement, one should carefully consider the associated losses due to the mere presence of a slot. If performance losses are deemed too large, care should be taken to seal or hide the slots in the cruise configuration.

Figure 6 shows the effect of introducing a total of six slots, two slots at the LEF shoulder, that is, at $x/c = 0.14$ and $x/c = 0.3$, and three sealed and one open slot on the TEF, on the pressure distribution and lift performance of the airfoil for a high-lift configuration. At incidence angles up to those corresponding to $C_{L,\max}$, that is, $\alpha = 13$ deg, there is no measurable effect on C_p or C_L of the airfoil. The TEF slots are not considered important at this TEF deflection because separation takes place at the TEF shoulder. Only the poststall performance ($\alpha = 14$ deg, Fig. 6) is affected in a measurable manner, due to the LEF actuator slots, especially the stalling slope. The sensitivity of the pressure distribution at poststall conditions to the LEF actuator slots indicates that they were machined in the right location to delay stall of the preceding configuration. At deep stall ($\alpha = 15$ deg), C_p is not altered by the presence of actuator slots.

Before control is applied, it is also necessary to determine where transition is occurring on the model to ensure that the control is not simply acting as an active BL trip. Laminar–turbulent transition on the LEF was detected using the hot-film information.[8,9] It is well established that laminar–turbulent transition is an intermittent process in which turbulent spots appear sporadically in time and from a rather narrow region in the streamwise direction. The spots are associated with a high-frequency content and a local alternation of the velocity profile from laminar to turbulent and vise versa (with a calming region following every mature spot).[10] The end result of these complex physical phenomena can be detected by a significant change in a single quantity, the standard deviation of the hot-film voltage (termed rms). Figure 7 presents the standard deviation of the hot-film voltages wrapped around the LEF for the landing configuration of Fig. 5 at $\alpha = 15$ deg. The stagnation point is marked by a slight increase in the rms associated with the meandering of the stagnation point in space and time. This occurs due to the TEF separated flow and vortex shedding process, which changes the circulation around the entire airfoil in a quasi-periodic manner. The cross correlation between adjacent sensors situated near the stagnation point indicates (as noted before[8,9]) the presence of a phase reversal due to the opposite wave propagation direction on the two sides of the stagnation point. Laminar–turbulent transition is evident from the large rms peak observed on the upper surface. The resolution of the hot film in space did not always allow for capturing this peak because it is a rather local phenomenon. Once transition occurred, the rms settles to a constant value, about twice the laminar rms, in agreement with the findings of Bertelrud.[8] Figure 7 indicates that transition occurs for the baseline case upstream of the excitation location, verifying that the excitation is not acting as a BL trip.

The effect of LEF separation control was initially studied with a small TEF deflection to allow reattachment to the entire airfoil upper surface with effective LEF control and to eliminate adverse effects due to unsteady interaction with the massively separated TEF flow, present at large TEF deflections.

Figure 8 shows the effect of the LEF deflection angle on the maximum lift coefficient of the airfoil at a fixed low TEF deflection for the baseline (with slots, no AFC) and for the optimally controlled airfoil by high-frequency excitation. Figure 9 presents baseline and controlled C_l–α curves, showing that a milder stall is gradually generated with a moderate increase in $C_{L,\max}$ due to the activation of the LEF actuator. For LEF deflections below -10 deg, the laminar flow separates at the LE, and, therefore, the activation of the LEF actuator (located at $x/c = 0.14$) is not effective. Once separation at high α is shifted to the LEF shoulder, the actuator delays stall by 1–2 deg and increases the maximum obtainable lift (Fig. 8) by about 12% at an LEF deflection of $\delta_s = -25$ deg. The actuator was operated near resonance, $f = 853$ Hz, for the preceding data set,

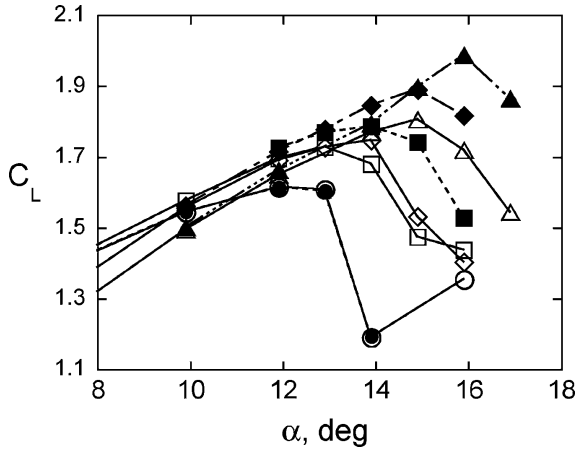

Fig. 9 Effect of slat deflection on the baseline and controlled lift, $\delta_f = 4.3$ deg, $Re_c = 0.75 \times 10^6$, both LE actuator slots used, $F^+ = 10.5$, and $C_\mu = 0.03\%$: ○, $\delta_s = 0$ deg, baseline; ◇, $\delta_s = -20$ deg, baseline; ●, $\delta_s = 0$ deg, control; ◆, $\delta_s = -20$ deg, control; □, $\delta_s = -15$ deg, baseline; △, $\delta_s = -25$ deg, baseline; ■, $\delta_s = -15$ deg, control; and ▲, $\delta_s = -25$ deg, control.

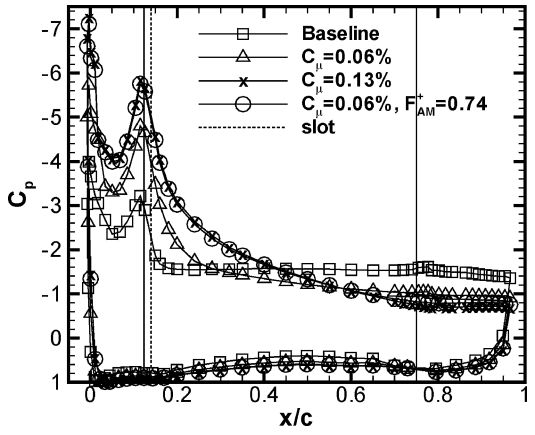

Fig. 10 Baseline and controlled C_p showing efficiency of $F^+_{AM} \sim 1$ actuation, $Re_c = 0.75 \times 10^6$, $\delta_f = 30$ deg, $\delta_s = -25$ deg, $\alpha = 15$ deg, $F^+ = 12.2$ when AM not applied.

resulting in an $F^+ = 10.5$, where length scale is the distance from the LEF $x/c = 0.14$ slot to the TE. It will be shown later that, by the use of AM, with an F^+_{AM} order of unity of the high-frequency excitation, one can obtain the same aerodynamic performance at one-half of the momentum input, saving at least 50% of the excitation energy.

From this point forward, the discussion will focus on the maximum lift condition for the airfoil, that is, $\delta_s = -25$ deg, $\delta_f = 30$ deg, and $\alpha = 15$ deg, for both the baseline and controlled cases. This flow condition was selected because it closely represents a high-lift landing configuration that will eventually also include TEF shoulder separation control.

Baseline and controlled pressure distributions for the preceding condition are presented in Fig. 10. The baseline flow separates downstream of the LEF shoulder at $x/c \approx 0.2$, based on the plateau of the pressure distribution. With AFC activated at the $x/c = 0.14$ slot, the flow reattaches to the main element and separates only at the TEF shoulder. Note that excitation with an AM signal generates almost the same pressure distribution, even though the C_μ was reduced by about 50% due to the modulation. (The peak slot exit velocity is the same.) The data shown in Fig. 10 also show that the use of a pure sine wave excitation, with a similar momentum coefficient as that of the AM signal, that is, $C_\mu = 0.06\%$, is significantly inferior. The wake surveys for the flow conditions of Fig. 10, provided in Ref. 11, indicate that, with control, the total drag is reduced very effectively, in agreement with the delayed separation on the airfoil.

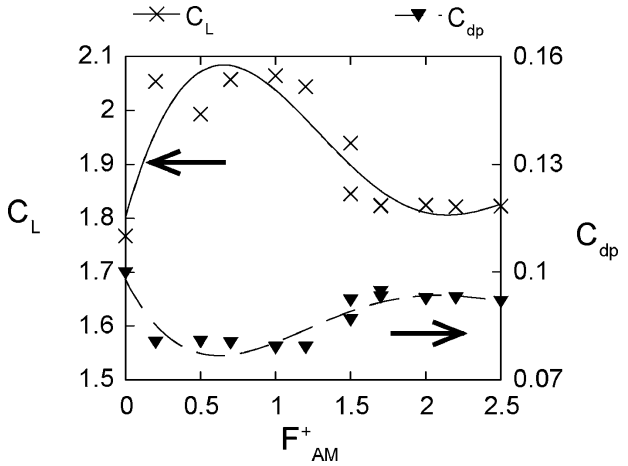

Fig. 11a Effect of F^+_{AM} on C_L and C_{dp}: $Re_c = 0.75 \times 10^6$, $\delta_f = 5$ deg, $\delta_s = -25$ deg, $C_\mu = 0.04\%$, and $\alpha = 15$ deg.

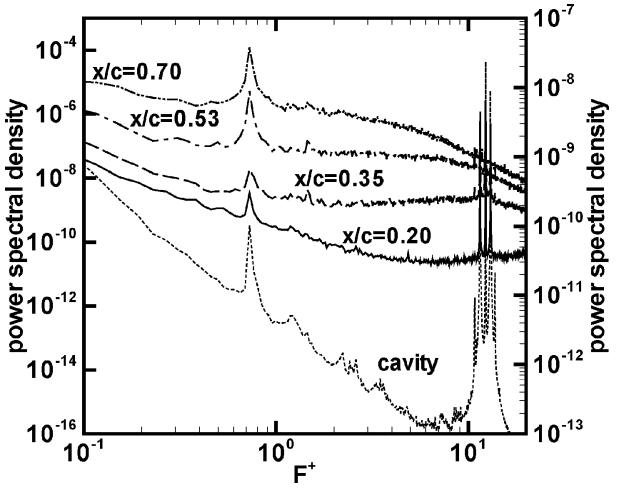

Fig. 11b Pressure spectra for the AM deg case of Fig. 10: $Re_c = 0.75 \times 10^6$, $\delta_f = 30$ deg, $\delta_s = -25$ deg, $F^+ = 12.2$, $F^+_{AM} = 0.74$, $C_\mu = 0.06\%$, and $\alpha = 15$ deg; right ordinate cavity pressure data, left ordinate all other data; all surface pressure spectra above $x/c = 0.20$ are shifted by a decade with respect to previous x/c.

The effect of the AM frequency f_{AM} on the airfoil performance was tested at a flow condition close to that of Figs. 8 and 9. The lift and form-drag variations due to the AM frequency are presented in Fig. 11a. The C_μ for these data is 0.04%. Note that the optimal lift increment and form-drag reduction are achieved at reduced frequencies in the range from 0.25 to 1.25. This is in good agreement with previous work utilizing flow instability for separation control[1,12,13] and excitation of a freejet,[14] even though the low-frequency excitation is strictly not present in the spectra of the actuator output. However, surface hot-film and fluctuating pressure data indicate that, further downstream of the actuator, the sidebands due to the AM (at $f_{res} \pm f_{AM}$) develop non-linearly into a distinct peak at f_{AM}. Figure 11b presents the spectra of the surface pressure fluctuations on the main element of the airfoil, corresponding to the AM data shown in Fig. 11a. Figure 11b also presents the spectrum of the actuator's cavity pressure fluctuations. The largest peak in both the cavity and $x/c = 0.2$ data is at $F^+ = 12.2$ (1 kHz), with two side bands at 12.2 ± 0.74, corresponding to the sum and difference between the actuator's resonant frequency and the AM frequency. The amplitude at the AM frequency (60 Hz) is almost three orders of magnitude smaller than the amplitude at resonance. Similar levels of pressure fluctuations were measured at $x/c = 0.2$ and 0.35 (where the excitation emanated from $x/c = 0.14$), whereas significant amplification of F^+_{AM} was measured at $x/c = 0.53$ and 0.6. Similar results were measured by the hot films, and quantitative differences due to the uncalibrated hot-film data and the surface quantity measured by the hot films with respect to the global nature of the surface

pressure fluctuations were noted. This finding indicates the existence of a nonlinear mechanism transforming the AM spectra and generating the low-frequency motion[15] that also coincides with the natural instability of the separating shear layer, amplifying the excitation. The data clearly show that excitation at an AM frequency that generates F^+_{AM} of order unity is very effective for separation control at the LEF shoulder. Margalit et al.[16] found that the separated shear layer on a delta wing was extremely receptive to an $F^+\mathcal{O}(1)$ AM signal and was completely insensitive to the high-frequency excitation, F^+ from 20 to 100, whereas even with AM no benefits were measured for $F^+_{AM} > 8$.

Figure 12 shows a comparison of the lift dependence on C_μ for the pure sine and AM excitation signals. The data clearly show that the $d(C_L)/d(C_\mu)$ slope for the AM is about twice that of the pure sine wave excitation, resulting in about a 50% reduction in the required C_μ for the same lift increment. The data do not show any indication of saturation, but the actuator's performance limits have been reached. Thus, no data are available at higher excitation levels.

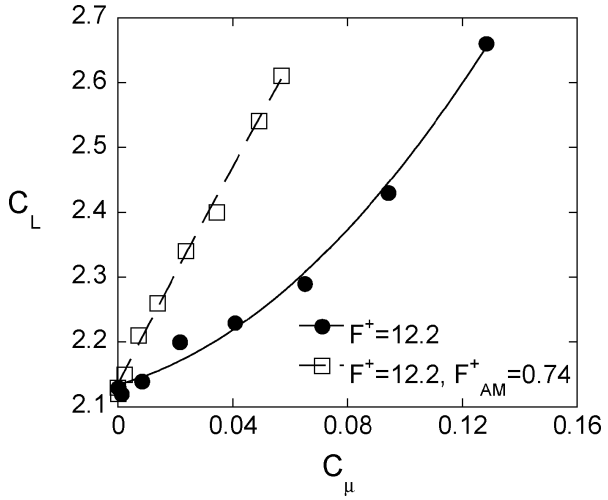

Fig. 12 Comparison of lift due to pure sine wave and AM sine wave excitation, $\alpha = 15$ deg, $\delta_s = -25$ deg, $\delta_f = 30$ deg, and $Re_c = 0.75 \times 10^6$.

a) Baseline

b) $F^+ = 12.2$, $F^+_{AM} = 0.74$, and $C_\mu = 0.06\%$

Fig. 13 Flow visualization images with light sheet produced by argon ion laser: $\delta_f = 30$ deg, $\delta_s = -25$ deg, $\alpha = 15$ deg, and $Re_c = 0.75 \times 10^6$.

Figures 13a and 13b show flow visualization images at conditions corresponding to the baseline and AM controlled C_p distributions of Fig. 10. The upper edge of the smoke plume does not follow the airfoil contour downstream of the LEF shoulder, indicative of flow separation in the baseline flowfield of Fig. 13a. With the application

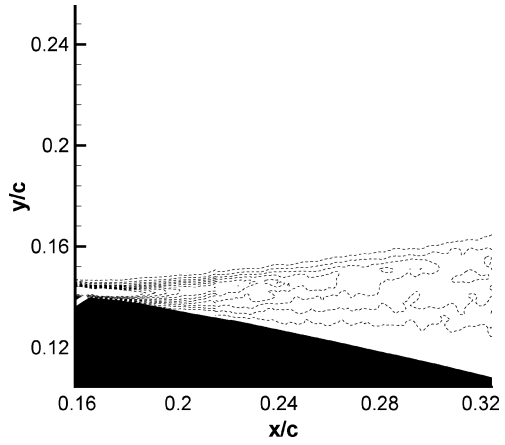

Fig. 14a Vorticity contours of baseline flowfield; vorticity normalized by U/c and contour increment 25, - - - -, negative vorticity: $\alpha = 15$ deg, $\delta_s = -25$ deg, $\delta_f = 30$ deg, and $Re_c = 0.75 \times 10^6$.

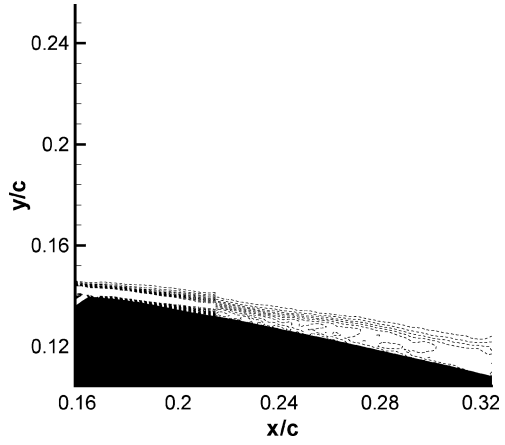

Fig. 14b Vorticity contours, $F^+ = 12.2$, $F^+_{AM} = 0.74$, and $C_\mu = 0.06\%$; vorticity normalized by U/c and contour increment 25, - - - -, negative vorticity; remaining parameters as in Fig. 14a.

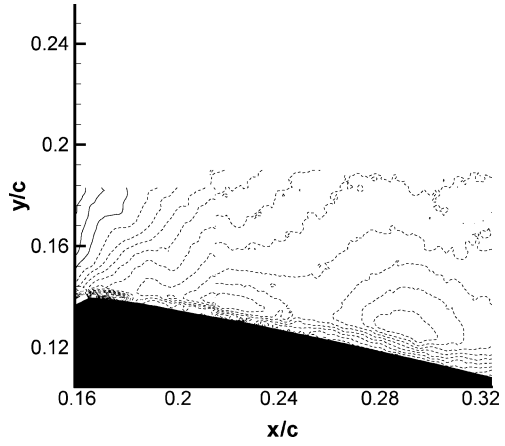

Fig. 14c PIV measured, phase-locked vertical component of velocity, $F^+ = 12.2$, $F^+_{AM} = 0.74$, and $C_\mu = 0.06\%$; contour level increment 1 m/s and - - - -, negative velocity; remaining parameters as in Figs. 14a and 14b.

of periodic excitation from the LEF shoulder, either with a pure sine wave or with a modulated sine wave (Fig. 13b), the flow reattaches and remains attached until the TEF shoulder. The reason for the flow reattachment is the generation of convectively unstable vortical structures that are not seen in the flow visualization images but that were measured by PIV and also by the hot films and unsteady pressure sensors downstream of the excitation slot.

Baseline and phase-locked controlled PIV data taken at the LEF shoulder region illustrate the significant change in the BL vorticity when the excitation was activated, focusing on the region close to the LEF actuator. The data also reveal the generation of coherent structures downstream of the excitation slots, even when a pure sine wave is used, for example, $F^+ \cong 12$. Figure 14a shows vorticity contours of the baseline flow, whereas Fig. 14b shows the same type of data for the AM signal controlled flow. The data from the two cameras used for the PIV overlap at $x/c = 0.21$, causing the discontinuity in the contour lines shown in Figs. 14. The coordinates shown in Figs. 14 are rotated by 15 deg, therefore, the LEF actuator slot at $x/c = 0.14$ is at $x/c = 0.163$. Good agreement was found between the baseline PIV, C_p, and hot-film data, indicating that the baseline flow separates between $x/c \cong 0.18$ and 0.2. When AM excitation is introduced from the $x/c = 0.14$ slot, an attached BL is restored (Fig. 14b). Figure 14c shows the phase-locked vertical component of velocity with a coherent downward directed momentum transferring velocity, in agreement with the hypothesis made by Seifert et al.[1] and Pack and Seifert.[12] Convectively unstable waves are seen to propagate downstream (Fig. 14c) with an initial wavelength of 5% chord. The wavelength increases as it progresses downstream. Note that these are the small-scale structures generated by the $F^+ = 12$ excitation. The large-scale structures resulting from the AM excitation and being amplified further cannot be seen in the small interrogation window.

Conclusions

Active separation control in the form of ZNMF oscillatory momentum injection was applied at the LEF shoulder of a supercritical airfoil. The LEF deflection increased the lifting capability of the airfoil by about 12%. The addition of periodic excitation roughly doubled that lift increment. Low-frequency AM modulation (with $F^+_{\mathrm{AM}} \cong 1$) of the high-frequency piezoelectric actuator output was used to save roughly 50% of the excitation momentum required to achieve the same performance gains. Separation was delayed to $x/c \cong 0.7$, with efficient LEF shoulder excitation. Future experiments will apply TEF separation control on the same airfoil and combinations of LEF and TEF excitations en-route to generating an efficient simplified high-lift system with comparable performance to the current three-element high-lift systems.

Acknowledgments

The authors would like to thank W. L. Sellers III, M. J. Walsh, A. E. Washburn, L. N. Jenkins, J. C. Lin, R. D. White, G. C. Hilton, J. Mau, L. M. Hartzheim, I. Fono, S. O. Palmer, R. D. Lewis, and A. R. McGowan.

References

[1]Seifert, A., Bachar, T., Koss, D., Shepshelovich, M., and Wygnanski, I., "Oscillatory Blowing: A Tool to Delay Boundary-Layer Separation," *AIAA Journal*, Vol. 31, No. 11, 1993, pp. 2052–2060.

[2]Seifert, A., and Pack, L. G., "Oscillatory Control of Separation at High Reynolds Numbers," *AIAA Journal*, Vol. 37, No. 9, 1999, pp. 1062–1071.

[3]McClean, J. D., Crouch, J. D., Stoner, R. C., Sakurai, S., Seidel, G. E., Feifel, W. M., and Rush, H. M., "Study of the Application of Separation Control by Unsteady Excitation to Civil Transport Aircraft," NASA/CR-1999-209338, June 1999.

[4]Lin, J. C., and Dominik, C. J., "Parametric Investigation of a High-Lift Airfoil at High Reynolds Numbers," *Journal of Aircraft*, Vol. 33, No. 4, 1997, pp. 485–491.

[5]Barlow, J. B., Rae, W. H., Jr., and Pope, A., *Low Speed Wind Tunnel Testing*, 3rd ed., Wiley, New York, 1999, pp. 328–366.

[6]Abbott, I. H., and van Doenhoff, A. E., *Theory of Wing Sections*, Dover, New York, 1949, pp. 227–231.

[7]Hoerner, S. F., and Borst, H. V., *Fluid-Dynamic Lift: Practical Information on Aerodynamic and Hydrodynamic Lift*, Hoerner Fluid Dynamics, L. A. Hoerner, Brick Town, NJ, 1975, pp. 5–4.

[8]Bertelrud, A., "Transition on a Three-Element High Lift Configuration at High Reynolds Numbers," AIAA Paper 98-0703, Jan. 1998.

[9]Nakayama, A., Stack, J. P., Lin, J. C., and Valarezo, W. O., "Surface Hot-Film Technique for Measurement of Transition, Separation, and Reattachment Points," AIAA Paper 93-2918, July 1993.

[10]Seifert, A., and Wygnanski, I., "On Turbulent Spots in a Laminar Boundary Layer Subjected to a Self-Similar Adverse Pressure Gradient," *Journal of Fluid Mechanics*, Vol. 296, Aug. 1995, pp. 185–209.

[11]Pack, L. G., Schaeffler, N. W., Yao, C. S., and Seifert, A., "Active Control of Separation from the Slat Shoulder of a Supercritical Airfoil," AIAA Paper 2002-3156, June 2002.

[12]Pack, L. G., and Seifert, A., "Effects of Sweep on the Dynamics of Active Separation Control," *Aeronautical Journal*, Vol. 107, No. 1076, 2003, pp. 617–629.

[13]Amitay, M., and Glezer, A., "Role of Actuation Frequency in Controlled Flow Reattachment Over a Stalled Airfoil," *AIAA Journal*, Vol. 40, No. 2, 2002, pp. 209–216.

[14]Wiltse, J. M., and Glezer, A., "Manipulation of Free Shear Flows Using Piezoelectric Actuators," *Journal of Fluid Mechanics*, Vol. 249, April 1993, pp. 261–285.

[15]Yehoshua, T., and Seifert, A., "Boundary Condition Effects on Oscillatory Momentum Generators," AIAA Paper 2003-3710, June 2003.

[16]Margalit, S., Greenblatt, D., Seifert, A., and Wygnanski, I., "Delta Wing Stall and Roll Control Using Segmented Piezoelectric Fluid Actuators," *Journal of Aircraft*, Vol. 42, No. 3, 2005, pp. 698–709.